



The 13th International Conference on Structural Safety and Reliability (ICOSSAR 2021-2022), Sept. 13-17, 2022, Shanghai, P.R. China

Path-Dependent Reliability and Resiliency of Critical Infrastructure via Particle Integration Methods

Roger Paredes, Hesam Talebiyan, and Leonardo Dueñas-Osorio

Department of Civil and Environmental Engineering, Rice University. E-mail: {roger.paredes, hesam.talebiyan, leonardo.duenas-osorio}@rice.edu.

Critical infrastructure is the backbone of modern societies. To meet increasing demand under resource-constrained and multihazard conditions, policy-makers are tapping into infrastructure resiliency: its capacity to withstand and recover from disruptions. Thus, resiliency-aware uncertainty quantification is key to identify tipping points, yet it remains computationally inaccessible. This paper maps resiliency measures to well understood time-dependent reliability computations, porting insights and methods from reliability theory to the service of critical infrastructure resiliency and upkeep efforts. For large-scale applications, we use *particle integration methods* (PIMs)—a family of sequential Monte Carlo methods with wide-ranging applications—and propose their optimal tuning in terms of their variance and number of limit-state function evaluations. We obtain consistent and unbiased probability estimates in applications to dynamical systems, network reliability, and resilience analysis, demonstrating PIMs as practical yet under-appreciated tools. For example, we obtain probability estimates of order 10⁻¹⁴ in networks with over 10,000 random variables.

Keywords: Dynamic, Reliability, Resiliency, Sequential Monte Carlo, Subset Simulation

1 INTRODUCTION

Critical infrastructure systems are becoming more complex and interconnected as the populations they serve grow more dependent on their continuous operation. Uncertainty quantification for such large-scale systems is imperative yet computationally prohibitive. For example, network reliability problems have no generally efficient solution (Ball, 1986). Thus, practical approximations continue to attract attention in engineering.

Alongside computational challenges, catastrophic events and natural disasters are unavoidable. Hence, engineering design across fields is expanding its focus from short-term efficiency to medium- and long-term resiliency (Ouyang et al., 2012;

Hosseini et al., 2016; Vardi, 2020). Thus, there is a need for principled uncertainty quantification techniques that, in alignment with the measurement sciences (Ellingwood et al., 2016), can quantify the tipping points of socio-technical regional systems and support decision making under uncertainty.

This paper extends the practicality of reliability methods to resiliency problems in critical infrastructure and beyond. Specifically, a generalization of the classical system reliability problem to the *path-dependent* setting makes it possible to treat relevant stochastic problems, including probabilistic resiliency, as a special case. Also, we use particle integration methods (PIM)¹ to give

¹We spell plural and singular acronyms the same.



practical and rigorous Monte Carlo approximations (Del Moral, 2013), deepening connections with known methods such as subset simulation (Au & Beck, 2001a). Building on past work, we put forward optimized PIM for unbiased uncertainty quantification and whose worst-case and best-case variances can be assessed in closed-form, behaving as crude Monte Carlo in the worst-case but exponentially more efficient under optimal conditions for practical applications. The unbiased property of estimates enables empirical verification of their performance in numerical simulations. The building blocks of PIM also set a research agenda for engineering problems, namely developing robust importance functions and efficient Markov Chain Monte Carlo (MCMC) samplers (Papaioannou et al., 2015; Wang et al., 2019).

The rest of the paper is as follows. Section 2 states the path-dependent reliability problem and shows that probabilistic resiliency is a special case. Section 3 introduces particle integration methods, and their optimized application to engineering problems, while connecting to subset simulation explicitly. Section 4 showcases applications to first-excursion probabilities, network and system reliability, and probabilistic resiliency. Section 5 summarizes our main results and conclusions, and outlines future research ideas.

2 PATH-DEPENDENT RELIABILITY

We state the problem of interest as computing the reliability of a path-dependent system, and show that it has probabilistic resilience as a special case. Afterwards, we discuss the computational complexity of the problem to motivate its sampling-based approximation.

2.1 The path-dependent reliability problem

We assume an *n*-dimensional system modeled as a stochastic process X(t), $0 \le t \le T$, that takes values in the state space \mathbb{R}^n . Let \mathscr{X} be the set of sample paths, or realizations of X. Then, we are interested in computing



The 13th International Conference on Structural Safety and Reliability (ICOSSAR 2021-2022), Sept. 13-17, 2022, Shanghai, P.R. China

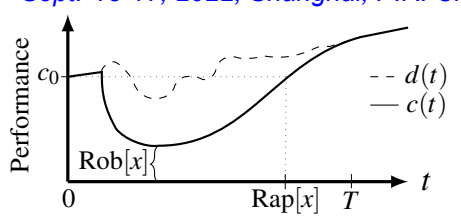


Figure 1. Demand (dashed) and capacity (solid) realization showing robustness (Rob) and rapidity (Rap).

the *path-dependent* system failure probability, which is written as an expectation over the set of sample paths

$$p_F := \mathbb{E}\{\mathbb{1}[g[X] \le 0]\} = \mathbb{P}\{g[X] \le 0\},$$
 (1)

where $g: \mathcal{X} \to \mathbb{R}$ is a limit-state *functional* (LSF) that maps sample paths to observables, in contrast to the limit-state *function* mapping system states to observables. Working with functionals allow us to specify time-dependent constraints, supporting stochastic problems like first-excursion probabilities (Au & Beck, 2001b) and probabilistic resilience (Hosseini et al., 2016). The classic system failure probability (Melchers & Beck, 2017, Section 1.5.3) applies as the static case T=0, i.e. X(0) is an n-dimensional vector of random variables (r.v.).

2.2 Special case: probabilistic resiliency

Consider the two-dimensional system X(t) = [C(t), D(t)], with time dependent capacity (*C*) and demand (*D*). Fig. 1 gives a pictorial representation of a sample path, or realization x(t) = [c(t), d(t)], of *X*.

Robustness-and-rapidity targets. Kameshwar et al. (2019) quantify resilience as the joint cumulative distribution function of robustness and rapidity

$$\overline{p_F} = \mathbb{P}\{\text{Rob}[X] \ge r_b, \text{Rap}[X] \le r_p\},\tag{2}$$

with robustness as the lowest capacity attained

$$Rob[x] = \min_{t \in [0,T]} c(t),$$



and rapidity the first-time of restoration

$$Rap[x] = \inf\{t \ge 0 : c(t) \ge c_0\},\$$

with respective targets r_b and r_p . For example, $r_b = c_0/2$ and $r_p = 0.7 \cdot T$.

For a highly-resilient system, without loss of generality, one is interested in a good approximation of *unresiliency* $p_F = 1 - \overline{p_F}$, which is the solution of a path-dependent reliability problem with LSF $g[x] = \min(\text{Rob}[x] - r_b, r_p - \text{Rap}[x])$.

Temporal average resilience. Ouyang et al. (2012) define the expected resilience ratio of a system as:

$$\mathbb{E}\{\mathbf{R}[X]\} = \mathbb{E}\left[\frac{\int_0^T C(t)dt}{\int_0^T D(t)dt}\right],\tag{3}$$

with $\int_0^T D(t) > 0$ for definiteness. Again, for a highly-resilient system, the expectation of R[X] is easy to approximate via crude Monte Carlo and, given a target average resiliency ratio r, we care for the unresiliency measure p_F with LSF g[x] = R[x] - r.

2.3 Computational intractability

For a polynomial-time LSF, computing p_F is #P-hard in general (Valiant, 1979), i.e. no generally efficient algorithm or analytical solution is believed to exists. Thus, there is significant interest in trustable probabilistic approximations (Karp et al., 1989) and stochastic simulation methods with variance reduction (Botev et al., 2012; Zuev et al., 2015; Vaisman et al., 2016; Cancela et al., 2019). We focus on the latter group of methods due to their scalability in real-world applications, and optimize particle integration methods (PIM) for engineering practice.

3 PARTICLE INTEGRATION METHODS

This section provides background on the Feynman-Kac model representation of the system reliability problem. The former is the archetypical model used in particle integration methods (PIM). Also, we give guidelines for the effective implementation of PIM.



The 13th International Conference on Structural Safety and Reliability (ICOSSAR 2021-2022), Sept. 13-17, 2022, Shanghai, P.R. China

3.1 Foundations and assumptions

We first layout the foundation to represent the system reliability problem as a Feynman-Kac model, which consists of an initial distribution, a sequence of Markov transition kernels, and a set of non-negative functions called potentials (more on Subsection 3.2).

For notation, we write '0:k' for '0,1,...,k' and ' $x_{0:k}$ ' for ' $(x_0,...,x_k)$.' Recall that a probability space $(\mathcal{X},\mathcal{F},\mathbb{P})$ consists of a sample space \mathcal{X} , a set of events \mathcal{F} , and a probability measure \mathbb{P} . Also, we use the measure-theoretic notation ' $\mathbb{P}(dx)$ ' ($\forall x \in \mathcal{X}$) instead of the probability density (or mass) function.

In particle integration methods, sample paths represent particle states.

Assumption 1 (Initial distribution) We can draw samples of X from the probability distribution $\mathbb{P}(dx)$, and the initial state of particles has the same distribution $M_0(dx) := \mathbb{P}(dx)$.

This assumption enables crude Monte Carlo (CMC) simulation, or simulating the initial state of a particle, denoted as $x_0 \in \mathcal{X}$. Particle integration methods consider sequences of sample paths (x_0, x_1, \ldots, x_k) , or particle trajectories, denoted as $x_{0:k} \in \mathcal{X}^{k+1}$. Hereafter, the subscript index l of x_l is called the trajectory index (Fig. 2).

Assumption 2 (MCMC sampler) We can sample transitions $X_l \sim M_l(x_{l-1}, \cdot)$ via Markov kernels M_l , l = 1:k, having \mathbb{P} as invariant measure.

We fulfill this assumption via Markov Chain Monte Carlo (MCMC) samplers, specially those that are robust in high-dimensional spaces (Papaioannou et al., 2015; Wang et al., 2019). In the theory of Markov processes, transition matrices can define conditional distributions in finite state spaces, whereas Markov kernels apply to more general spaces.

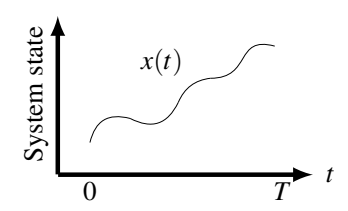
Remark 1 A random trajectory has probability distribution:

$$\mathbb{M}_k(dx_{0:k}) = M_0(dx_0) \prod_{l=1}^k M_l(x_{l-1}, dx_l),$$





The 13th International Conference on Structural Safety and Reliability (ICOSSAR 2021-2022), Sept. 13-17, 2022, Shanghai, P.R. China



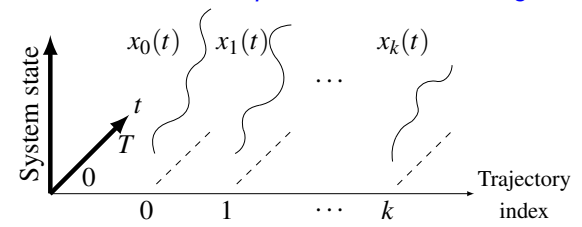


Figure 2. (Left) System sample path $x \in \mathscr{X}$ with probability distribution $\mathbb{P}(dx)$ considered in CMC. (Right) Particle trajectory $x_{0:k} \in \mathscr{X}^{k+1}$ with probability distribution $\mathbb{M}_k(dx_{0:k})$ considered in PIM.

and every kernel having \mathbb{P} as invariant measure means that the initial distribution is preserved, i.e. $X_l \sim M_0(\cdot)$, l = 0:k.

Thus, in contrast to standard MCMC applications, no burn-in is needed to reach the target (initial) distribution, and later we show this suffices to sample (sequentially) from the conditional distribution $\mathbb{P}(\cdot|F)$, $F \subseteq \mathcal{X}$ (Subsection 3.3). However, correlation between particle transitions can increase the variance of estimates and 'burn-in' can indeed mitigate it (Cérou et al., 2012).

Assumption 3 (Importance function) We have access to a functional $L : \mathscr{X} \to \mathbb{R}$ such that $L[x] \ge 1$ if and only if $g[x] \le 0$.

The importance function is also referred to as the reaction coordinate in molecular dynamics (Cérou et al., 2011). In our setting, the importance function is a smooth analog of the failure indicator function $\mathbb{1}[g[X] \leq 0]$. When the LSF is such that g[X] has a continuous cumulative distribution function (c.d.f.) we can adopt L[x] = 1 - g[x]. However, for general cases, choosing the ideal importance function remains an open problem (Bréhier & Lelièvre, 2019). Subsection 4.3 tackles the case of a network with discrete random variables.

We are now ready to map the system reliability problem to the computation of the partition function of a Feynman-Kac model.

3.2 Feynman-Kac model

Given a sequence of nonnegative functions, $G_k: \mathscr{X} \to [0, \infty), k \in [1:K)$, called potentials,

and a Markov process $X_{0:K}$, the Feynman-Kac model is given by the change of probability measure from \mathbb{M}_K (Del Moral, 2013; Chopin & Papaspiliopoulos, 2020):

$$\mathbb{Q}_{K}(dx_{0:K}) = \frac{1}{Z_{K}} \left[\prod_{k=1}^{K} G_{k}(x_{k}) \right] \mathbb{M}_{K}(dx_{0:K}),$$
(4)

with *partition function* (normalizing constant):

$$Z_K = \mathbb{E}_{\mathbb{M}_K} \left[\prod_{k=1}^K G_k(X_k) \right] > 0, \tag{5}$$

Intuitively, the product of nonnegative potentials assigns a weight to every particle trajectory, and the partition function Z_K is the sum of all such weights.

To cope with the computational intractability of partition functions, an approach dating back to Kahn & Harris (1951) writes a telescoping product

$$\frac{Z_K}{Z_0} = \frac{Z_1}{Z_0} \frac{Z_2}{Z_1} \cdots \frac{Z_K}{Z_{K-1}},\tag{6}$$

so that every ratio is "easy" to approximate. Indeed, several independently developed algorithms for approximating ratios, e.g. adaptive multilevel splitting (Botev & Kroese, 2012; Turati et al., 2016) and Subset Simulation (Au & Beck, 2001a), can be interpreted as the *interacting* particle integration method that follows. Consider an ensemble of particles $x_k^j \in \mathcal{X}$, with trajectory index k = 0:K, particle index j = 1:N, and initial state distribution $X_0^j \sim M_0(\cdot)$. Then, for each k = 1:K and j = 1:N, sample the transition $X_k^j \sim M_k(x_{k-1}^p, \cdot)$ choosing p with rate



 $G_k(x_{k-1}^p)/\sum_{i=1}^N G_k(x_{k-1}^i)$, which is the key interaction between particles. Finally, use the ensemble of particles $x_{0:K}^{1:N}$ to approximate the partition function Z_K .

While most engineering studies build upon subset simulation (e.g. Wang et al., 2019), we adopt the super set of particle integration methods. The latter includes consistent and unbiased probability estimation algorithms in terms of the mean and variance (Botev et al., 2012; Cérou et al., 2012), which we tune to the practically relevant case of a costly LSF.

3.3 Back to path-dependent reliability

To express the failure probability p_F [Eq. (1)] as the partition function Z_K , introduce a sequence of nested sets $F_0 \supset \cdots \supset F_K$, with $F_k = \{L[X] \geq L_k\}$ and importance scores $-\infty = L_0 < \cdots < L_K = 1$. Note that $p_F = \mathbb{P}(F_K)$. Then, setting the potentials G_k equal to $\mathbb{1}_{F_k}$ gives the sought after Feynman-Kac model, with partition function $Z_K = p_F$.

For the case of a binary potential, a particle transitions from $x_{k-1} \in F_k$ to x_k obeying the 'conditional' kernel

$$M_k^*(x_{k-1}, dx_k) = M_k(x_{k-1}, \bar{F}_k) \mathbb{1}(x_{k-1} = x_k) + M_k(x_{k-1}, dx_k) \mathbb{1}_{F_k}(x_k),$$
(7)

having $\mathbb{P}(\cdot|F_k)$ as invariant measure, and mirroring the final "accept or reject" step in MCMC samplers for reliability analysis (Papaioannou et al., 2015, Section 3). Also, from Bayes rule, the ratios become

$$\frac{Z_k}{Z_{k-1}} = \frac{\mathbb{P}(F_k)}{\mathbb{P}(F_{k-1})} = \mathbb{P}(F_k|F_{k-1}) =: p_k, \quad (8)$$

showing that subset simulation (Au & Beck, 2001a) is a special case of the partition function ratios of a Feynman-Kac model.

In practice, we encounter highly reliable and resilient systems ($p_F < 10^{-4}$), making crude Monte Carlo impractical. Thus, the importance scores $L_{0:K}$ are chosen so that the conditional probabilities p_k are easy to approximate. When LSF evaluations are computationally intensive, Subsection 3.5 gives evidence in support of $p_k \approx 0.2032$.



The 13th International Conference on Structural Safety and Reliability (ICOSSAR 2021-2022), Sept. 13-17, 2022, Shanghai, P.R. China

The success of particle integration methods hinges on their effective implementation.

3.4 Computer implementations

The next algorithms differ from typical implementations in two aspects, they use 'conditional' transition kernels M_k^* [Eq. (7)] and avoid bootstrap resampling of particles. This choice improves algorithmic performance when the kernels M_k have slow mixing time (Botev & Kroese, 2012), while having no impact on the theoretical best-case performance of PIM.

Annealed PIM. We call the first algorithm due to Botev & Kroese (2012) the annealed particle integration method (aPIM, Algorithm 1) in analogy to the process of controlled heating and cooling of materials. Importantly, aPIM returns an unbiased estimate of p_F assuming the importance scores (inverse temperatures) $L_{0:K}$ are known. In practice, we run Algorithm 2 (introduced later), but return $L_{0:K}$.

Algorithm 1 aPIM (Botev & Kroese, 2012)

```
Input: Scores L_{0:K}, initial distribution M_0, kernels
       M_{1\cdot K}^*, and splitting factor s = 5 (recommended).
  1: Set \mathbf{X}_k \leftarrow \emptyset, k = 1:K,
 2: Set \mathbf{X}_0 \leftarrow \{X \sim M_0(\cdot)\}.
 3: for k \in [1:K) do
 4:
             for Y_0 ∈ \mathbf{X}_{k-1} : L[Y_0] \ge L_k do
 5:
                   for j = 1:s do
                         Sample Y_j \sim M_k^*(Y_{j-1}, \cdot).
 6:
                         Set \mathbf{X}_k \leftarrow \mathbf{X}_k \cup \{Y_i\}.
 7:
 8:
                   end for
 9:
             end for
10: end for
11: Set \mathbf{X}_K \leftarrow \{x \in \mathbf{X}_{K-1} : L[x] \ge 1\}
12: return \hat{p_F}^{aPIM} = |\mathbf{X}_K|/s^{K-1}.
```

Using *N* iterations of aPIM we get the next unbiased approximations of the mean and variance of the failure probability estimator (adapted from Botev & Kroese, 2012):

$$\hat{\mu}_N = \frac{s^{-(K-1)}}{N} N_K = \frac{s^{-(K-1)}}{N} \sum_{i=1}^N |\mathbf{X}_K^j|, \qquad (9)$$

$$\hat{\sigma}_N^2 = \frac{s^{-2(K-1)}}{N(N-1)} \sum_{i=1}^N \left(|\mathbf{X}_K^j| - \frac{N_K}{N} \right)^2, \quad (10)$$



with splitting factor $s = 1/p_k$. Also, we have the next bounds on the *relative variance*² of aPIM (Botev & Kroese, 2012):

$$\sum_{k=1}^{K} \frac{1 - p_k}{p_k} \le \frac{\sigma_{\text{aPIM}}^2}{(p_F)^2} \le \frac{1}{p_F} - 1,\tag{11}$$

where the upper bound matches the performance of crude Monte Carlo and holds for perfectly correlated particle transitions, whereas the lower bound holds for a perfectly mixing kernel, i.e. independent transitions.

Interacting PIM. The second algorithm, called the interacting particle integration method (iPIM, Algorithm 2), computes the importance scores $L_{0:K}$ on-the-fly, but returns a biased failure probability estimate (Cérou et al., 2012). The key interaction among particles is through the importance scores $L_{0:K}$ (Lines 4 and 14).

Adaptive-levels methods such as Algorithm 2 (iPIM) and subset simulation present challenges. For example, Botev & Kroese (2012) observe bias accompanied by underestimation of the relative variance in large scale problems. However, $\hat{p_F}^{\text{iPIM}}$ is *positively* biased and of order 1/N, which partially mitigates the issue, and Cérou et al. (2012) give a correction of the bias for the *ideal* case of a perfectly mixing kernel, where the relative variance becomes $(N \rightarrow \infty)$

$$N\frac{\sigma_{\text{iPIM}}^2}{(p_F)^2} = n_0 \frac{1 - p_0}{p_0} + \frac{1 - r_0}{r_0},\tag{12}$$

with $p_0 = 1/s$, $n_0 = \lfloor \frac{\log p_F}{\log p_0} \rfloor$ and $r_0 = p_F p_0^{-n_0}$. Next, we empirically show that the ideal

Next, we empirically show that the ideal performance of the previous algorithms converges asymptotically. This insight motivates tuning algorithms to the practical case of a computationally expensive LSF, as in critical infrastructure systems.

3.5 Annealed or interacting? Better together

For perfectly mixing kernels and conditional failure probabilities $p_k = 1/s$, $k \in [1:K)$,



The 13th International Conference on Structural Safety and Reliability (ICOSSAR 2021-2022), Sept. 13-17, 2022, Shanghai, P.R. China

Algorithm 2 iPIM (Cérou et al., 2012)

Input: Initial distribution M_0 , kernels $M_{k>0}^*$, number of particles N, and splitting factor s=5 (recommended) multiple of N.

```
1: Set q \leftarrow N(1-1/s)
 2: Sample \mathbf{X}_0 = \{X_0^j \sim M_0(\cdot) : j = 1:N\}
 3: Sort \mathbf{X}_0 increasing in L_0^j = \mathbf{L}[X_0^j]
 4: Set L_1 \leftarrow (L_0^q + L_0^{q+1})/2 and k \leftarrow 0
 5: while L_{k+1} < 1 do
               Set k \leftarrow k+1 and \mathbf{X}_k \leftarrow \emptyset
for Y_0 \in X_{k-1}^{q:N} do
 7:
                      for j = 1:s do
 8:
                             Sample Y_j \sim M_k^*(Y_{j-1}, \cdot)
 9:
10:
                              \mathbf{X} \leftarrow \mathbf{X}_k \cup \{Y_i\}
11:
               end for Sort L_k^{j-1} < L_k^j = L[X_k^j], \ j = 2:N. Set L_{k+1} \leftarrow (L_k^{q-1} + L_k^q)/2.
12:
13:
14:
15: end while
                                                                        ▶ Need for aPIM
16: L_{k+1} \leftarrow 1
17: \mathbf{X}_{k+1} \leftarrow \{X_k^j \in \mathbf{X}_k : L_k^j \ge 1\}.
18: return \hat{p_F}^{\text{iPIM}} = s^{-k} |\mathbf{X}_{K+1}| / N
```

aPIM and iPIM have asymptotically the same variance [Eq. (12)] and make the same number of LSF evaluations in expectation, denoted #g. We verified this empirically in one dimension and found that, while $p_k = 1/2$ results in the smallest variance [Fig. 3(left)], the choice $p_k^* \approx 0.2032$ minimizes the *inef*ficiency, defined as $\Delta^2 = \sigma^2/p_F^2 \times \#g$, which can be interpreted as the expected number of LSF evaluations required to produce an estimate with 'unit coefficient-of-variation' (Au et al., 2007). Specifically, assuming integer $K = \log(p_F)/\log(p_k)$, the minimization of $\Delta^2 = K^2(1 - p_k)/p_k$ has a closed-form solution in terms of the Lambert W function when p_k is equal to $-W(-2/e^2)/2 \approx 0.2032$. Thus, we choose s = 5, and pursue efficient importance functions and kernels approaching the ideal performance of iPIM.

The similar asymptotic behavior of iPIM and aPIM motivates our dual approach. First, run iPIM choosing N as large as possible to obtain importance scores $L_{0:K}$ that minimize the variance of aPIM. Then, use aPIM to obtain a consistent and unbiased variance estimate $\hat{\sigma}_N^2$ whose true value is equal or greater than the variance of iPIM.

²Proportional to the number of samples to rigorously approximate p_F (Paredes et al., 2019).



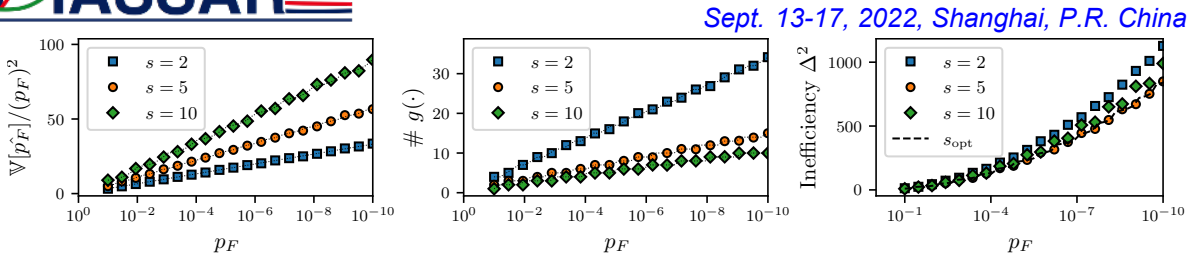


Figure 3. Idealized one-dimensional example. Plots show analytical and empirical values of the (left) relative variance, (center) expected number of LSF calls, and (right) inefficiency. Dotted lines show predicted values for iPIM and markers show aPIM results; which are in stark agreement.

4 NUMERICAL EVALUATION

We fix $N = 10^5$ and s = 5 for all experiments (Algorithms 1 and 2). Typically, subset simulation studies need independent runs to obtain a sample mean (biased) and variance. Instead, we use N samples of aPIM and a single run of iPIM and obtain unbiased estimates $\hat{\mu}_N$ (mean) and $\hat{\sigma}_N^2$ (variance). Thus, like with crude Monte Carlo, we can compute approximate 99% normal confidence intervals, denoted $CI_N(99\%)$, which are asymptotically correct $(N \to \infty)$; however, they do not guarantee correct approximations in the finite sample regime (e.g. Paredes et al., 2019). For the conditional kernels M_t^* in Algorithms 1 and 2, we use the preconditioned Crank-Nicolson (pCN) of Cotter et al. (2013) and the Modified Metropolis-Hastings (MMH) of Au & Beck (2001a). The former is used in Hamiltonian Monte Carlo (Wang et al., 2019, Eq. (21)) and similarly competitive MCMC samplers (Papaioannou et al., 2015, Subsection 3.3).

We evaluate the empirical performance of PIM in terms of the coefficient of variation, or the inefficiency Δ^2 when the exact value of p_F is known. The optimal inefficiency Δ^2_* is calculated for a perfectly mixing kernel and optimal splitting factor $1/s_{\rm opt} \approx 0.2032$.

Our empirical validation includes Gaussian models with known closed-form solutions. Thus, in the reminder of this section we let $\xi \sim \mathcal{N}(0,1)$ be a standard normal r.v. with c.d.f. ϕ . Also, B is the standard Brownian motion with B(0) = 0 and $B(t+s) - B(s) \sim \mathcal{N}(0,t)$ for all t,s>0, and W is white noise given by $B(t) := \int_0^t W(t) dt$.

Table 1. Linear limit-state function ($\kappa = 0$).

β	p_F	CI _N (%99)	$ar{\Delta}^2/\Delta_*^2$
Z 2 4 6	2.28×10^{-2} 3.17×10^{-5} 9.87×10^{-10}	$(2.26\pm0.11)\times10^{-2}$ $(3.18\pm0.33)\times10^{-5}$ $(9.41\pm1.38)\times10^{-10}$	2.55 3.93 3.30
HWW 6	2.28×10^{-2} 3.17×10^{-5} 9.87×10^{-10}	$(2.26\pm0.10)\times10^{-2}$ $(3.12\pm0.30)\times10^{-5}$ $(9.20\pm1.47)\times10^{-10}$	2.00 3.44 3.65

We use test-cases to challenge the performance of particle integration methods.

4.1 *Linear/nonlinear limit state function*

First, we consider a limit-state function with a parameterized nonlinearity and known closed-form solution to assess the robustness of estimates in a high-dimensional problem. The limit-state function is defined as:

$$g(x) = \beta - \frac{\kappa}{4}(x_1 - x_2)^2 - \frac{1}{\sqrt{n}} \sum_{i=1}^{n} x_i,$$

with $x_i \sim \mathcal{N}(0,1)$, i=1:n, and exact solution p_F independent of n (Papaioannou et al., 2015, Eq. (34)). For $\kappa=0$ the limit-state function is linear and $p_F=\phi(-\beta)$. Tables 1 and 2 show results for n=1000. The pCN and MMH kernels had comparable performance and their inefficiency Δ^2 was roughly 2-8 times greater than the optimal.

4.2 Random vibration

This example consists of a single-barrier problem that has no closed-form solution, and we show that PIM issues a much more efficient approximation than Crude Monte



Table 2. Nonlinear limit-state function ($\beta = 4$).

κ	p_F	CI _N (%99)	$\bar{\Delta}^2/\Delta_*^2$
-0.2 -1.0 5.0	8.99×10^{-3}	$(9.04\pm0.59)\times10^{-3}$	4.01 3.48 5.17
HH -0.2 -1.0 5.0	8.99×10^{-3}	$(8.99\pm0.51)\times10^{-3}$	3.01 2.53 6.49

Table 3. Random vibration example.

	a/σ_T	$p_F(\approx)$	CI _N (%99)	$\bar{\sigma}/\bar{\mu}$
pCN	3.0 4.0 5.0	$\begin{array}{c} 6.01 \times 10^{-2} \\ 1.79 \times 10^{-3} \\ 1.97 \times 10^{-5} \end{array}$	$(5.68\pm0.21)\times10^{-2}$ $(1.85\pm0.14)\times10^{-3}$ $(2.05\pm0.22)\times10^{-5}$	0.01 0.02 0.03
MMH	3.0 4.0 5.0	$\begin{array}{c} 6.01 \times 10^{-2} \\ 1.79 \times 10^{-3} \\ 1.97 \times 10^{-5} \end{array}$	$(5.64\pm0.18)\times10^{-2}$ $(1.83\pm0.12)\times10^{-3}$ $(2.12\pm0.20)\times10^{-5}$	0.01 0.02 0.03

Carlo, while guaranteeing consistent and unbiased estimates. Consider a single-degree-of-freedom oscillator subject to white noise:

$$\ddot{X}(t) + 2\zeta\omega\dot{X}(t) + \omega^2X(t) = \sqrt{\omega}W(t),$$

$$X(0) = \dot{X}(0) = 0,$$

with $\omega = 2\pi \operatorname{rad/s}$, $\zeta = 0.02$, and the LSF $g[x] = T - \tau_A$, with $\tau_A = \inf\{t : x(t) \ge a\}$ and $T = 15 \operatorname{s}$, i.e. p_F is the probability that X(t) will exit threshold a before time T. Assuming a time-domain discretization of the white noise, the response becomes

$$X(t_i) \approx \sum_{j=0}^{300} h(t_i - t_j) \xi_j \sqrt{2\pi\Delta t}, \quad i = 0.300,$$

 $h(t) = \mathbb{1}(t \ge 0) \cdot e^{-\zeta \omega t} \omega_d^{-1} \sin(\omega_d \cdot t),$

with $t_i = i\Delta t$, $\Delta t = 0.05 \, \mathrm{s}$ and $\omega_d = \omega \sqrt{1 - \zeta}$. Table 3 shows results for various thresholds a, with approximate reference values of p_F and response standard deviation σ_T from Au & Beck (2001b, Table 1 and Eq. (44)). The reference values come from crude Monte Carlo $(N=10^6)$ and are in rough agreement with our unbiased approximations despite having a greater coefficient of variation.



The 13th International Conference on Structural Safety and Reliability (ICOSSAR 2021-2022), Sept. 13-17, 2022, Shanghai, P.R. China

4.3 *Network reliability*

This example demonstrates the applicability of PIM in discrete domain problems. We adapt a latent-variable model (Botev et al., 2012). First, for every binary r.v. that takes value zero with probability $p_i = \phi^{-1}(-\beta_i)$, introduce a standard normal r.v. $X_i \sim \mathcal{N}(0,1), i = 1:n$. The binary r.v. can be expressed as $Y_i(t) = \mathbb{1}(X_i + 1 - \beta_i \leq t)$, for t = 1. Then, we use as importance function

$$L[x] = \inf\{t \in \mathbb{R} : g[y(t)] \le 0\},\tag{13}$$

which makes at most $\log_2(n)$ calls to the LSF $g: \{0,1\}^n \to \mathbb{R}$ using binary search. Recall that the importance function is a smooth analog of the failure indicator function. It is known that $p_F = \mathbb{P}\{L[X] > 1\}$. The transformation to the standard normal space allow us to use pCN/MMH with a single call to the importance function per kernel sample. Instead, the competitive Gibbs sampler of Botev et al. (2012) makes n calls per kernel sample.

We focus on the multiterminal network unreliability problem: for a graph G = (V, E), compute the probability that a specified set of terminals $V' \subseteq V$ becomes disconnected given that each edge $e \in E$ fails independently with probability p_e . Here, $g[\cdot] = 1$ if the terminals are connected and $g[\cdot] = 0$, otherwise.

We consider the square lattice 100×100 with 10000 vertices and 19800 edges. For the case of two terminals in opposing corners, one can obtain a lower bound as reference value using exact sequential bounding techniques (e.g. Paredes et al., 2018). In this example we use $N = 10^4$, as storing N vectors of size 19800 takes roughly 1.5 gigabytes using double floating-point representation. Table 4 shows estimates that are in agreement with the reference values. To the best of our knowledge, state-of-the-art methods struggle with similar instances in the rareevent regime. For example, Ching & Hsu (2007, Table 1) consider the same example but crude Monte Carlo outperforms their estimates using standard graph traversal algorithms such as breadth-first-search. Also, the method of Zuev et al. (2015) does not address



Table 4. Network reliability (100×100 grid).

	p_e	$p_F (\geq)$	$CI_N(\%99)$	$ar{\sigma}/ar{\mu}$
bCN	1e-03 1e-05 1e-07	$2 \times 10^{-6} \\ 2 \times 10^{-10} \\ 2 \times 10^{-14}$	$(1.90\pm0.76)\times10^{-6}$ $(2.23\pm1.10)\times10^{-10}$ $(2.62\pm1.46)\times10^{-14}$	0.12 0.15 0.17
MMH	1e-03 1e-05 1e-07	$2 \times 10^{-6} 2 \times 10^{-10} 2 \times 10^{-14}$	$(2.07\pm1.03)\times10^{-6}$ $(2.57\pm3.53)\times10^{-10}$ $(2.06\pm2.25)\times10^{-14}$	0.15 0.42 0.33

the importance function so it is not directly applicable to a binary LSF such as in connectivity reliability.

4.4 Probabilistic resiliency

We consider a network flow restoration model of the power transmission network of Shelby County, TN (González et al., 2016), and compute its unresiliency p_F : the probability of violating robustness or rapidity constraints [Eq. (2)]. The recovery model mirrors an iterative mixed integer program that, given a budget per unit of time (e.g. repairs per day), identifies the network elements whose repair maximize demand satisfaction. The power network data consist of 75 nodes (9 supply nodes and 42 demand nodes) and 93 transmission lines. This network system is substantially smaller than the previous due to the intractability of the LSF, which requires solving an iterative mixed integer program. We assume independent transmission line outages with uniform probabilities of failure, and a single outage repair per unit of time; however, it is straightforward to consider pairwise correlations or hazard-andsite specific fragilities. To test the efficiency of our approach, we consider various values of the transmission line failure probability p_e , rapidity target r_p (time horizon) and robustness target r_b (satisfied demand).

We use the latent variable formulation from the previous section and, given a sample path x, consider a copy $x^{(j)}$ for each time unit $j = 0, 1, \ldots$, with $x_i^{(j)} = -\infty$ if network element i is repaired by time unit j. The importance



The 13th International Conference on Structural Safety and Reliability (ICOSSAR 2021-2022), Sept. 13-17, 2022, Shanghai, P.R. China

function in this case is:

$$L[X] = \max(L_{Rob}[X^{(0)}], L_{Rap}[X^{(Rap[X])}]),$$

where L_{Rob} (resp. L_{Rap}) is like Eq. (13), but we have $g[\cdot] \le 0$ when the satisfied demand is less than r_b (resp. 100%).

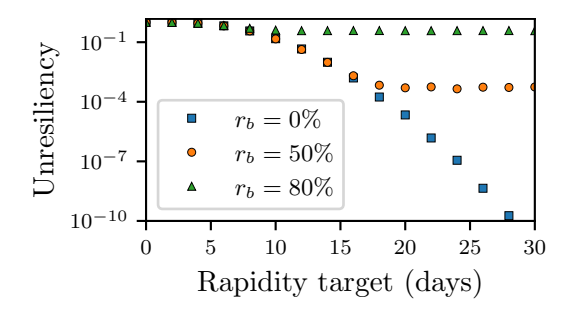


Figure 4. Unresiliency for various recovery targets.

Fig. 4 shows results for $p_e = 1/10$. When $r_p = 0$ and $r_b = 80\%$, the system does not tolerate drops of satisfied demand after the disruption, and the system is highly unresilient. As the rapidity and robustness constraints are less stringent, the system transitions into highly-resilient, and the computation of p_F is infeasible via crude Monte Carlo methods. Clearly, enhancing only system robustness, or rapidity, sets a ceiling on how much we can reduce unresiliency. To the best of our knowledge, our approach gives the first consistent and unbiased estimation of failure probabilities in highly-resilient systems.

5 CONCLUSIONS

We considered the path-dependent system reliability problem and its application to firstexcursion probabilities, network reliability, and the probabilistic resiliency of critical infrastructure systems.

We optimized the performance of Particle Integration Methods (PIM) to engineering applications with computationally expensive limit-state functions. The main advantage over traditional algorithms, e.g. subset simulation, is that ours deliver consistent and unbiased estimates. Using a wide range of numerical examples, we empirically verified near-optimal performance in practice, with ineffi-



ciency values within an order of magnitude of the optimal performance.

For future research, we are studying rigorous approximations guaranteeing user-specified relative error and confidence parameters. Also, we are studying efficient Markov Chain Monte Carlo samplers and importance functions for applications of interest, including random excitation of non-linear structures and the joint-decentralized recovery of critical infrastructure systems.

6 Acknowledgments

The authors gratefully acknowledge the support by the U.S. National Institute of Standards and Technology (Grant 70NANB20H008).

7 REFERENCES

- Au, S. K. & Beck, J. L. 2001a. Estimation of small failure probabilities in high dimensions by subset simulation. Probabilistic Engineering Mechanics, 16(4), 263–277.
- Au, S. K. & Beck, J. L. 2001b. First excursion probabilities for linear systems by very efficient importance sampling. Probabilistic Engineering Mechanics, 16(3), 193–207.
- Au, S. K., Ching, J., & Beck, J. L. 2007. Application of subset simulation methods to reliability benchmark problems. Structural Safety, 29(3), 183–193.
- Ball, M. O. 1986. Computational Complexity of Network Reliability Analysis: An Overview. IEEE Transactions on Reliability, 35(3), 230–239
- Botev, Z. I. & Kroese, D. P. 2012. Efficient Monte Carlo simulation via the generalized splitting method. Statistics and Computing, 22(1), 1–16.
- Botev, Z. I., L'Ecuyer, P., Rubino, G., Simard, R., & Tuffin, B. 2012. Static Network Reliability Estimation via Generalized Splitting. INFORMS Journal on Computing, 25(1), 56–71.
- Bréhier, C.-E. & Lelièvre, T. 2019. On a new class of score functions to estimate tail probabilities of some stochastic processes with adaptive multilevel splitting. Chaos: An Interdisciplinary Journal of Nonlinear Science, 29(3), 033126.
- Cancela, H., Murray, L., & Rubino, G. 2019. Efficient Estimation of Stochastic Flow Network Reliability. IEEE Transactions on Reliability, 1–17.
- Cérou, F., Del Moral, P., Furon, T., & Guyader, A. 2012. Sequential Monte Carlo for rare event estimation. Statistics and Computing, 22(3), 795–808.
- Cérou, F., Guyader, A., Lelièvre, T., & Pommier, D. 2011. A multiple replica approach to simulate reactive trajectories. The Journal of Chemical Physics, 134(5), 054108.
- Ching, J. & Hsu, W.-C. 2007. An Efficient Method for Evaluating Origin-Destination Connectivity Reliability of Real-World Lifeline Networks. Computer-Aided Civil and Infrastructure Engineering, 22(8), 584–596.
- Chopin, N. & Papaspiliopoulos, O. 2020. An Introduction to Sequential Monte Carlo, Vol. 52 of Springer Series in Statistics. Springer International Publishing, Cham (dec).
- Cotter, S. L., Roberts, G. O., Stuart, A. M., & White, D. 2013. Mcmc methods for functions: Modifying old algorithms to make them faster. Statistical Science, 28(3), 424–446.



The 13th International Conference on Structural Safety and Reliability (ICOSSAR 2021-2022), Sept. 13-17, 2022, Shanghai, P.R. China

- Del Moral, P. 2013. Mean Field Simulation for Monte Carlo Integration. Chapman and Hall/CRC (may).
- Ellingwood, B. R., van de Lindt, J. W., & McAllister, T. P. 2016. Developing measurement science for community resilience assessment. Sustainable and Resilient Infrastructure. 1(3-4), 93–94.
- González, A. D., Dueñas-Osorio, L., Sánchez-Silva, M., & Medaglia, A. L. 2016. The Interdependent Network Design Problem for Optimal Infrastructure System Restoration. Computer-Aided Civil and Infrastructure Engineering, 31(5), 334–350.
- Hosseini, S., Barker, K., & Ramirez-Marquez, J. E. 2016. A review of definitions and measures of system resilience. Reliability Engineering and System Safety, 145, 47–61.
- Kahn, H. & Harris, T. E. 1951. Estimation of particle transmission by random sampling. National Bureau of Standards applied mathematics series, 12, 27–30.
- Kameshwar, S., Cox, D. T., Barbosa, A. R., Farokhnia, K., Park, H., Alam, M. S., & van de Lindt, J. W. 2019. Probabilistic decision-support framework for community resilience: Incorporating multi-hazards, infrastructure interdependencies, and resilience goals in a Bayesian network. Reliability Engineering and System Safety, 191(July), 106568.
- Karp, R. M., Luby, M., & Madras, N. 1989. Monte-Carlo approximation algorithms for enumeration problems. Journal of Algorithms, 10(3), 429–448.
- Melchers, R. E. & Beck, A. T. 2017. Structural Reliability Analysis and Prediction. John Wiley & Sons Ltd, Chichester, UK (oct).
- Ouyang, M., Dueñas-Osorio, L., & Min, X. 2012. A three-stage resilience analysis framework for urban infrastructure systems. Structural Safety, 36-37, 23–31.
- Papaioannou, I., Betz, W., Zwirglmaier, K., & Straub, D. 2015. MCMC algorithms for Subset Simulation. Probabilistic Engineering Mechanics, 41, 89–103.
- Paredes, R., Dueñas-Osorio, L., & Hernandez-Fajardo, I. 2018. Decomposition algorithms for system reliability estimation with applications to interdependent lifeline networks. Earthquake Engineering & Structural Dynamics, 47(13), 2581–2600.
- Paredes, R., Dueñas-Osorio, L., Meel, K. S., & Vardi, M. Y. 2019. Principled network reliability approximation: A countingbased approach. Reliability Engineering & System Safety, 191, 106472
- Turati, P., Pedroni, N., & Zio, E. 2016. Advanced RESTART method for the estimation of the probability of failure of highly reliable hybrid dynamic systems. Reliability Engineering and System Safety, 154, 117–126.
- Vaisman, R., Kroese, D. P., & Gertsbakh, I. B. 2016. Splitting sequential Monte Carlo for efficient unreliability estimation of highly reliable networks. Structural Safety, 63, 1–10.
- Valiant, L. G. 1979. The Complexity of Enumeration and Reliability Problems. SIAM Journal on Computing, 8(3), 410–421.
- Vardi, M. Y. 2020. Efficiency vs. resilience. Communications of the ACM, 63(5), 9–9.
- Wang, Z., Broccardo, M., & Song, J. 2019. Hamiltonian Monte Carlo methods for Subset Simulation in reliability analysis. Structural Safety, 76, 51–67.
- Zuev, K. M., Wu, S., & Beck, J. L. 2015. General network reliability problem and its efficient solution by Subset Simulation. Probabilistic Engineering Mechanics, 40, 25–35.